

Numerical simulation of Kelvin-Helmholtz instability using an implicit, non-dissipative DNS algorithm

This article has been downloaded from IOPscience. Please scroll down to see the full text article.

2011 J. Phys.: Conf. Ser. 318 032024

(<http://iopscience.iop.org/1742-6596/318/3/032024>)

View [the table of contents for this issue](#), or go to the [journal homepage](#) for more

Download details:

IP Address: 193.140.147.132

The article was downloaded on 29/03/2013 at 14:21

Please note that [terms and conditions apply](#).

Numerical simulation of Kelvin-Helmholtz instability using an implicit, non-dissipative DNS algorithm

İ Yılmaz¹, L Davidson², F O Edis³ and H Saygın⁴

¹ Energy Institute, Istanbul Technical University, Maslak, Istanbul, Turkey

² Division of Fluid Dynamics, Department of Applied Mechanics, Chalmers University of Technology, Gothenburg, Sweden

³ Faculty of Aeronautics and Astronautics, Istanbul Technical University, Maslak, Istanbul, Turkey

⁴ Faculty of Engineering and Architecture, Istanbul Aydın University, Florya, Istanbul, Turkey

E-mail: yilmazily@itu.edu.tr

Abstract. An in-house, fully parallel compressible Navier-Stokes solver was developed based on an implicit, non-dissipative, energy conserving, finite-volume algorithm. PETSc software was utilized for this purpose. To be able to handle occasional instances of slow convergence due to possible oscillating pressure corrections on successive iterations in time, a fixing procedure was adopted. To demonstrate the algorithm's ability to evolve a linear perturbation into nonlinear hydrodynamic turbulence, temporal Kelvin-Helmholtz Instability problem is studied. KHI occurs when a perturbation is introduced into a system with a velocity shear. The theory can be used to predict the onset of instability and transition to turbulence in fluids moving at various speeds. In this study, growth rate of the instability was compared to predictions from linear theory using a single mode perturbation in the linear regime. Effect of various factors on growth rate was also discussed. Compressible KHI is most unstable in subsonic/transonic regime. High Reynolds number (low viscosity) allows perturbations to develop easily, in consistent with the nature of KHI. Higher wave numbers (shorter wavelengths) also grow faster. These results match with the findings of stability analysis, as well as other results presented in the literature.

1. Introduction

Kelvin-Helmholtz Instability (KHI) occurs when a perturbation is introduced into a system with a velocity shear (Batchelor, 1967). It is subject to many physical and engineering topics such as turbulent mixing, astrophysical jets and aerodynamic wake flows. Linear stability theory can be used to predict the onset of instability and transition to turbulence for such flows. The *dispersion relation* which relates growth of the instability (ω_g) to wave number (k_x) is given by stability analysis as $\omega_g = k_x \frac{\sqrt{\rho_1 \rho_2}}{\rho_1 + \rho_2} |\Delta v|$ for inviscid and incompressible flows with an infinitesimally thin shear layer where ρ_1 and ρ_2 are densities and Δv is velocity difference between layers. k_x is $2\pi/\lambda$ where λ is wavelength. Growth is directly proportional to wave number in the direction of the flow so that smaller waves grow faster. This is also valid for compressible flows. Michalke (1964) studied hyperbolic tangent velocity profile and showed that fastest growing modes are the ones whose wavelength is comparable to shear layer thickness a , $k_x a \approx 1$. Blumen (1970) extended this study to compressible flows and found that shear layer is unstable, when Mach

number ($M = v_0/c_s$) is between 0 and $\sqrt{2}$ where v_0 is initial freestream velocity and c_s is speed of sound. Mach number for the most unstable case was also predicted as $\sqrt{3}/2$.

In this study, growth rate of the instability is studied using an implicit, non-dissipative, direct numerical simulation (DNS) algorithm proposed by Hou & Mahesh (2005). For this purpose, an in-house fully parallel DNS solver based on this algorithm was developed using PETSc (Balay et al, 1997). Effects of different Mach numbers, Reynolds numbers (Re) and wave numbers on the development of the instability in terms of growth rate are discussed. Results are compared to linear theory, as well as results those available in literature.

Rest of the paper is organized as follows. In section 2, algorithm is reviewed and its parallelization is briefly explained. In section 3, the code is applied to KHI with random mode perturbations in order to demonstrate the ability of the algorithm to evolve a linear perturbation into nonlinear hydrodynamic turbulence. Single mode KHI problem is solved and growth rate is discussed in section 4. In the last section, conclusions are made and paper is finalized.

2. Numerical method

2.1. The base algorithm

Present DNS study is based on the algorithm of Hou & Mahesh (2005). This is an implicit, non-dissipative, predictor-corrector type, second-order, cartesian finite volume algorithm. It solves fully compressible Navier-Stokes equations for an ideal gas. Incompressible pressure scaling is used in order to handle low-Mach number flows properly. Unlike many other methods, face-normal velocities (V_N) are calculated by projection. Variables are co-located in space and staggered in time. Face values are found by simple averaging. These features make the algorithm discretely energy conserving, robust, non-dissipative, and applicable to flows with a wide range of Mach numbers.

Especially at low Mach numbers, we observed oscillating pressure-corrections (dp 's) in our test runs which is caused to slow convergence on successive iterations in time. To remedy this, a procedure suggested by Walton (1989) was adopted into our code.

2.2. Parallelization of the code

In order to study large problems with an implicit algorithm, parallelization is essential. DNS code developed in this study uses the Portable, Extensible Toolkit for Scientific Computation (PETSc). PETSc is a suite of data structures and routines that provide the building blocks for the implementation of large-scale application codes on parallel computers (Balay et al, 1997). PETSc uses distributed memory parallelism which is based on the message-passing interface (MPI) for communication. It includes a suite of parallel linear solvers which can be chosen even in run-time. Distributed Arrays (DAs) context is designed to handle problems on structured grids. DAs decompose domain, as well as objects such as vectors and matrices and perform all necessary communications among the available processors.

Since boundary condition support for DAs is limited in the stable release of PETSc, we implement non-periodic boundary conditions into a parallel PETSc in the following way. First, DAs are defined to have periodic boundary conditions in all directions. Then, ghost cells reserved for the periodicity are used to store necessary values for non-periodic boundaries.

Linear systems arising from discretization are solved by using *ILU(0)-preconditioned GMRES* algorithm. Parallel runs were performed on 256 cores.

3. KHI simulations with random mode perturbations

We consider here three-layer subsonic slip surface setup of three-dimensional KHI. This is the same one used in tests of Athena code (Stone et al, 2008) in 2D, except density stratification.

Domain sizes are $-0.5 \leq x \leq 0.5$, $-0.5 \leq y \leq 0.5$, and $-0.5 \leq z \leq 0.5$. Three-layer setup allows us to use periodic boundary conditions for all directions. Initial streamwise velocity (u_0) is set to -0.5 for $|y| > 0.25$ and 0.5 for $|y| \leq 0.25$. Velocities in other directions are set to zero. Uniform initial pressure ($p_0 = 2.5$) and density ($\rho_0 = 1$) profiles are used. Ratio of specific heats (γ) is taken as 1.4, giving a Mach number of 0.267. Prandtl number is 0.72 and Reynolds number based on domain length, velocity difference, and dynamic viscosity of air is around 6.10^4 . Dynamic viscosity is related to temperature via power-law, $\mu(T) = T^{0.67}$. 128^3 grid is chosen for simulation. Time step is set to 10^{-3} for all simulations. To trigger instability, random

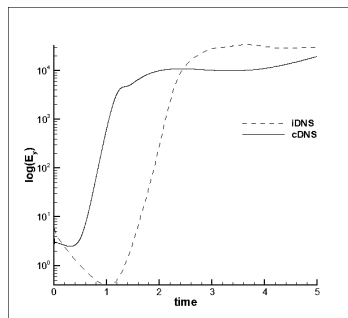


Figure 1. Development of the y -component of total kinetic energy for random mode perturbation

mode perturbations are added both to streamwise (u) and to normal velocity (v) components within intermediate layer. Form of the perturbation is $A_0(\text{rand}(\text{iseed}) - 0.5)$ where A_0 is the amplitude which is set to 0.01 and iseed is the random number variable taken as 1. We followed the development of the instability up to non-linear regime where $t_{\text{end}} \approx 5.0$.

Figure 1 shows evolution of the y -component of total kinetic energy (E_y), in comparison to results obtained by the incompressible DNS ($iDNS$) algorithm of Davidson & Peng (2003). Growth of instability follows three steps within linear range; a settling period, an exponential growth, and saturation phase. Qualitative picture given by the methods are as expected by the linear theory and comparable to results calculated by Athena code (Stone et al, 2008) and Fyris Alpha code (Sutherland, 2010). Although saturation levels are almost same, growth time scales are very different. Differences in the growth times can be related to different dissipative characteristics of the methods. Due to inherent dissipation included by scheme, settling period may take more time on the same grid resolution, as it is observed in the results obtained by Athena and Fyris Alpha. In figure 2, development of instability is shown in terms of iso-surfaces of span-wise component of vorticity (ω_z). Earlier growth of instability is predicted by current non-dissipative DNS ($cDNS$) algorithm. Through the end of the linear regime, flow gradually approaches to transition to turbulence, which is predicted by both methods.

4. KHI simulations with single mode perturbations

The aim of this test is to compare numerical results obtained by $cDNS$ algorithm with the growth rate derived from the linear perturbation analysis. All cases were initialized with a hyperbolic tangent velocity profile for streamwise velocity, $u(y) = v_0 \tanh\left(-\frac{y}{a}\right)$ where a is initial shear layer thickness and is set to 0.05. This value is small enough to avoid boundary effects. Upper and lower boundaries are located at $10a$. v_0 is used to change Mach number and will be specified. Other velocity components are set to zero. Upper and lower streams have opposite v_0 velocities. Initial pressure and density fields are uniform which are $p_0 = 1/\gamma$, and $\rho_0 = 1$ respectively. These initial conditions are same with those used in ZEUS code of Clarke (1996). Convective

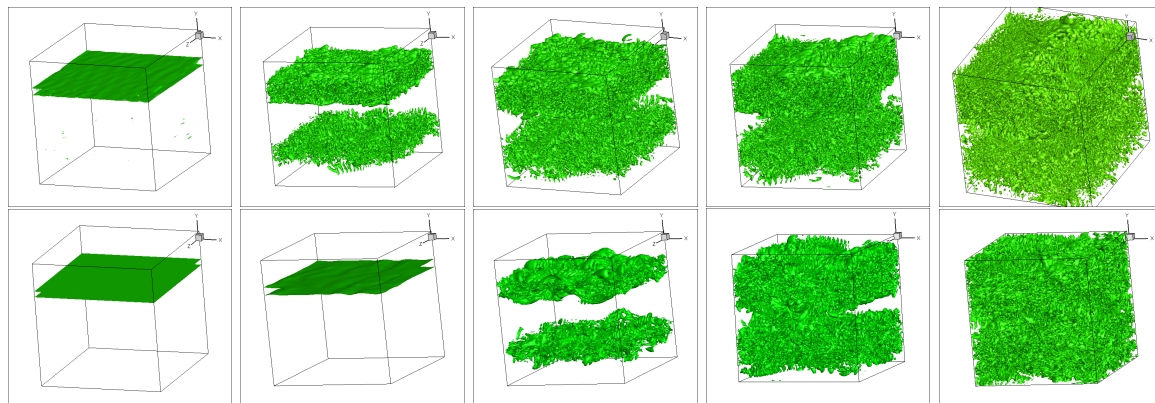


Figure 2. Iso-surfaces of spanwise vorticity ($\omega_z = 1$) calculated by cDNS(top) and iDNS(bottom) at $t=1,2,3,4,5$ from left to right.

Mach number (M_c) introduced in Bogdanoff (1983) and Papamoschou & Roshko (1998) is given as, $M_c = \frac{\Delta v}{c_{s1} + c_{s2}}$ where c_{s1} and c_{s2} are speeds of sound of each layer. Since speeds of sound are same for given initial conditions, which is fixed to unity, M_c is equal to Mach number M for all cases and is taken as reference Mach number M_r into our code. Prandtl number is 0.72 and specific ratio of heats is 1.4, as in the previous section. Domain is between -0.5 and 0.5 in all directions. Resolution is chosen as 256^3 . Flow is followed up to $t_{end} \approx 10.0$ with a fixed time step, 10^{-3} . Normal velocity component is perturbed with a single-mode perturbation in

Table 1. Simulation parameters and results

Case	M_s	Re	k_x	v_0	δ_{w0}	$\Gamma a/v_0$	$2E_{max}/\rho_0 v_0^2$
M1	0.250	1409	2π	0.250	0.1	0.092	244.66
M2	0.375	2114	2π	0.375	0.1	0.120	186.10
M3	0.500	2819	2π	0.500	0.1	0.138	109.07
M4	0.625	3523	2π	0.625	0.1	0.146	70.13
M5	0.750	4228	2π	0.750	0.1	0.097	43.55
M6	0.875	4933	2π	0.875	0.1	0.085	33.84
M7	1.000	5638	2π	1.000	0.1	0.073	21.54
W1	0.750	4228	π	0.750	0.1	0.098	43.49
W2(M5)	0.750	4228	2π	0.750	0.1	0.097	43.55
W3	0.750	4228	2.5π	0.750	0.1	0.095	43.36
W4	0.750	4228	3π	0.750	0.1	0.088	42.97
R1(M1)	0.250	1409	2π	0.250	0.1	0.092	244.66
R2	0.250	28090	2π	0.250	0.1	0.166	346.47
R3	0.250	100000	2π	0.250	0.1	0.171	347.08

the form, $\delta v_y = v_{y0} \sin(k_x x) \exp(-y^2/\sigma^2)$. Amplitude is taken as $v_{y0} = 0.01$ which is smaller than v_0 for all cases. σ represents the decay of the amplitude in the outer region $|y| > a$, and the ratio σ/a is set to 4. λ is taken as domain length. Boundary conditions in the y -direction are adiabatic slip walls where face normal velocity V_N is zero. Other boundaries are periodic.

Following Keppens et al (1999) and Miura and Pritchett (1982), growth rate, Γ , is determined

by monitoring the y -component of total kinetic energy, $E_y = \iiint (\rho v^2/2) dx dy dz$, which is calculated by summing up values over whole domain. Saturation level E_{max} is the first maximum of $E_y(t)$ at time t . The corresponding time is also defined as t_{max} . $E_y(t)$ then is fitted to an exponential, $\exp(2\Gamma t)$, within the time interval of $[0.25t_{max}, 0.4t_{max}]$. $\Gamma a/v_0$ is used for comparison.

Mach number effects are studied by changing Δv at fixed $k_x = 2\pi$. For wave number cases, M is set to 0.75. Reynolds number is based on average density, velocity difference, and half initial vorticity thickness (δ_{w0}). Initial vorticity thickness is given as $\delta_{w0} = \frac{\Delta v}{|du/dy|_{max}}$. $M = 0.25$ and $k_x = 2\pi$ are also chosen to demonstrate the effects of Reynolds numbers on growth rate. In this case, different length scales are used to study with different Re 's. Table 1 summarizes the important simulation parameters and results for all cases. Cases with M, W, and R denote Mach number, wave number and Reynolds number study respectively. In figure 3.a, development

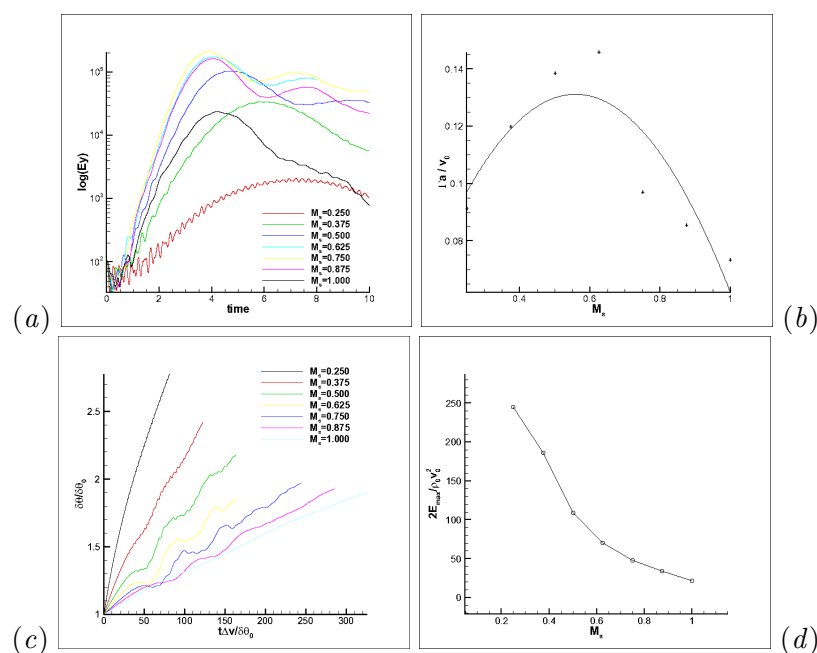


Figure 3. Change of y -component of total kinetic energy(a), growth rate(b), saturation level(c) and momentum thickness(d) with Mach number

of E_y in time is plotted for different Mach numbers. Reynolds numbers are approximately in the same order, therefore their effects on results should be equal and it can be ignored for this comparison. We will also evaluate how really Reynolds number effects the results at $M = 0.25$ later on. Instability develops hardly both at lower and higher values. Under quasi-incompressible conditions where densities are equal and velocity difference is small, this is the predicted behavior by linear theory. In figure 3.b, polynomial fitting is also performed over the growth rates obtained by the procedure defined before. Resulting curve is similar to Keppens et al (1999). Mach number where the highest growth rate observed is around 0.625. Although this is slightly less than given by theory, it is the same result obtained with ZEUS code. A small deviation is due to non-zero thickness of shear layer. Decrease in the momentum thickness, $\delta\theta = \int_0^\infty \frac{\rho(y)u(y)}{\rho_0 u_0} (1 - \frac{u(y)}{u_0}) dy$, with increasing Mach number is shown in figure 3.c. This evolution matches to figure 2 of Pantano & Sarkar (2002). Saturation levels show a similar characteristic with increasing Mach number, in consistent with figure 8 of Keppens et al (1999).

Comparison of E_y for different wave numbers is given in figure 4.a. Figure 4.b also compares normalized growth rates. $k_x a$ where the highest growth rate occurs is around 0.2 at $M = 0.75$.

For incompressible case, this value is given as ≈ 0.45 . Keppens et al (1999) found ≈ 0.4 for $M = 0.5$. As Miura & Pritchett (1982) explained, wave number of the fastest growing mode is shifted to smaller values with increasing Mach number, in agreement with results in Blumen (1970). Saturation levels in figure 4.c are decreasing with increasing wave number, similar to figure 7 in Keppens et al (1999).

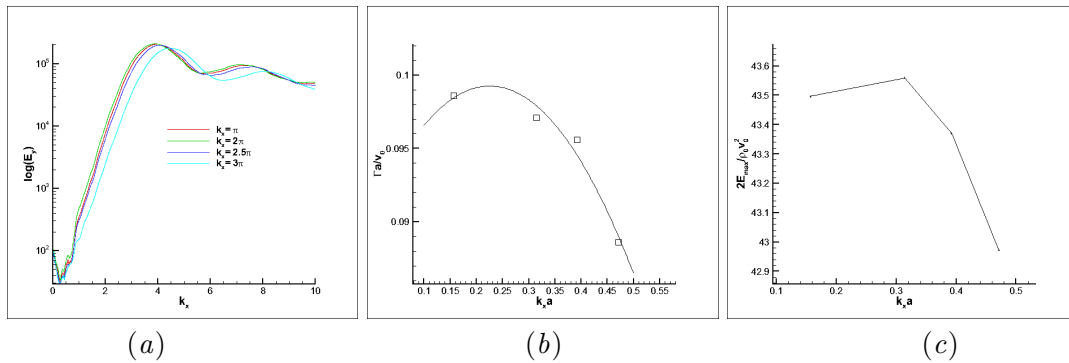


Figure 4. Change of y-component of total kinetic energy(a), growth rate(b), and saturation level(c) with wave number

We also performed runs to show effects of Reynolds number on development of instability at $M = 0.25$, which is the $M1$ case that instability develops hardly. As it is seen in figure 5, when flow is getting closer to inviscid conditions, instability develops smoothly in compared to low Reynolds number case, which is consistent with the inviscid nature of KHI. Growth rates and saturation levels do not change noticeably at higher Reynolds numbers. These results are also consistent with critical Reynolds number given by Dimotakis (2005) for a mixing layer instability to evolve turbulence.

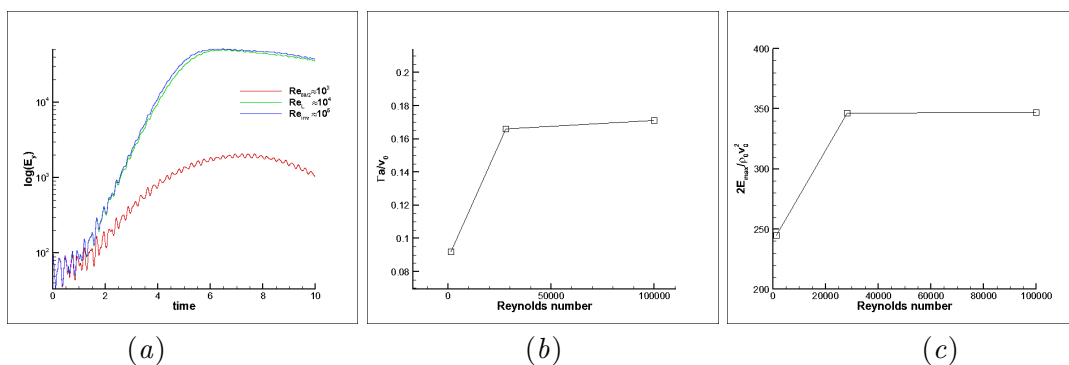


Figure 5. Change of y-component of total kinetic energy(a), growth rate(b), and saturation level(c) with wave number

5. Conclusions

We developed a fully parallel DNS solver based on a non-dissipative, implicit algorithm which conserves kinetic energy discretely. Solver was applied to KHI problem where linear perturbation evolves into nonlinear hydrodynamic turbulence. We showed that algorithm is able to capture physics of such kind of transitional flows. Effect of various factors such as Mach number, Reynolds number and wave number on the development of the instability were also discussed.

Random case results showed that inherent dissipation included by scheme has stabilizing effect on the instability. Single mode runs were performed in order to compare results to theory, as well as previous numerical results. Mach number regime where instability is most unstable found by the algorithm is subsonic/transonic regime, as predicted by the stability analysis. Most unstable wave numbers are getting decrease to smaller values with an increasing Mach number. Decreasing viscosity (high Re) allows perturbations to develop smoothly. Since KHI is an inviscid problem, this is an expected result as also pointed out by some previous studies.

Detailed studies using the non-dissipative DNS solver with initial turbulent velocity fields to understand the physical mechanisms of mixing transition to turbulence at high Mach numbers for compressible turbulent shear layers can also be considered as a further research topic.

Acknowledgments

This study is financially supported by Istanbul Technical University (ITU) and The Scientific and Technological Research Council of Turkey (TUBITAK). Computing resources used in this work were provided by the National Center for High Performance Computing of Turkey (UYBHM) under grant number 1001212011 and Center for Scientific and Technical Computing in Chalmers University of Technology in Sweden, under the Project SNIC001-10-22.

References

- BALAY S., GROPP W. D., MCINNES L. C. & SMITH B. F. 1997 Efficient management of parallelism in object oriented numerical software libraries. *Modern Software Tools in Scientific Computing*. (ed. E. Arge, A. M. Bruaset & H. P. Langtangen), 163–202.
- BATCHELOR, G. K. 1967 *An Introduction to Fluid Dynamics* (Cambridge: Cambridge University Press).
- BLUMEN, W. 1970 Shear layer instability of an inviscid compressible fluid. *J. Fluid Mech.* **40**, 769.
- BOGDANOFF, D. 1983 Compressibility effects in turbulent shear layers. *AIAA J.* **21**, 926–927.
- CLARKE D. A. 1996 A consistent method of characteristics for multidimensional magnetohydrodynamics. *Astrophys. J.* **457**, 291–320.
- DAVIDSON, L. & PENG S. H. 2003 Hybrid LES-RANS: a one-equation SGS model combined with a k-omega model for predicting re-circulating flows. *Int. J. Num. Meth. In Fluids.* **43**, 1003–1018.
- DIMOTAKIS P. E. 2005 Turbulent mixing. *Annu. Rev. Fluid Mech.* **37**, 329–356.
- HOU, Y. & MAHESH K. 2005 A robust, colocated, implicit algorithm for direct numerical simulation of compressible, turbulent flows. *J. Comp Phys.* **205**, 205–221.
- KEPPENS K., TÓTH G., WESTERMANN R. H. J. & GOEDBLOED, J. P. 1999 Growth and saturation of the Kelvin-Helmholtz instability with parallel and anti-parallel magnetic fields. *J. Plasma Phys.* **61**, 1–19.
- MICHALKE, A. 1964 On the inviscid instability of the hyperbolic tangent velocity profile. *J. Fluid Mech.* **19**, 543.
- MIURA A. & PRITCHETT. P. L. 1982 Nonlocal stability analysis of the mhd Kelvin-Helmholtz instability in a compressible plasma. *J. Geophys. Res.* **87**, 7431–7444.
- PANTANO, C. & SARKAR, S. 2002 A study of compressibility effects in the high-speed turbulent shear layer using direct simulation. *J. Fluid Mech.* **451**, 329–371.
- PAPAMOSCHOU, D. & ROSHKO, A. 1988 The compressible turbulent shear layer: an experimental study. *J. Fluid Mech.* **197**, 453–477.
- STONE J. M., GARDINER T. A., TEUBEN P., HAWLEY J. F. & SIMON J. B. 2008 Athena: a new code for astrophysical magnetohydrodynamics. *The Astrophys. J. Suppl. Series.* **178**, 137–177.
- SUTHERLAND, R. S. 2010 A new computational fluid dynamics code I: Fyris Alpha. *Astrophys. & Space Sci.* **327**, 173–206.
- WALTON G. N. 1989 Airflow network models for element-based building airflow modeling. *ASHRAE Transactions.* **95**, 613–620.